Available online at www.sciencedirect.com

ScienceDirect

Procedia Engineering 109 (2015) 356 – 363

Procedia Engineering

www.elsevier.com/locate/procedia

XXIII Italian Group of Fracture Meeting, IGFXXIII

Full field strain measurement of dissimilar laser welded joints

Giovanni Battista Broggiato[a], Luca Cortese[b], Filippo Nalli[b], Pasquale Russo Spena[b]*

[a]*Mechanical and Aerospace Engineering Department, Sapienza University of Rome, Via Eudossiana 18, Roma 00184, Italy*
[b]*Faculty of Science and Technology, Free University of Bozen-Bolzano, P.zza Università 5, Bolzano 39100, Italy*

Abstract

Laser welded tailored-blanks (TWBs) made of dissimilar advanced high strength steel (AHSS) sheets are used in the automotive industry to produce resistant and lightweight components. However, the stamping of AHSS TWBs poses some issues concerning the different formability of the parent materials and of the weld seams. Moreover, the weldment exhibits an inhomogeneous mechanical behavior due to the presence of a fusion zone and of a heat affected zone. For this reason, it is crucial to be able to assess the local mechanical properties of the welded joints in order to optimize the laser welding parameters for the fabrication of AHSS TWBs, and hence to guarantee proper formability of TWBs in the final stamping process. In this paper, digital image correlation is employed to investigate the mechanical properties of laser welded joints. Overall and local behavior are studied by means of two image acquisition systems working at different magnification levels and framing the front and the back side of a loaded specimen in a tensile test. The use of two image grabbing systems has been introduced to measure the strain field as close as possible to the weld seam where high strain gradients are present. To this purpose, it has been necessary to tune the parameters of the image correlation processing algorithm. This is because the method, working on image subsets on which the displacement field is modeled with low order shape functions, leans to smooth displacement gradients and strain singularities. By varying post-processing parameters an elaboration strategy has been suggested to capture the strain gradients correctly. The approach, here applied to laser welded joints, may be also used to measure the surface strain field wherever defects or inhomogeneity create strain discontinuities.

Peer-review under responsibility of the Gruppo Italiano Frattura (IGF)

Keywords: resistance spot welding; advanced high strength steels, white light speckle correlation, local deformation field

* Corresponding author. Tel.: +33-0471-017-112-; fax: +33-0471-017-646
E-mail address: pasquale.russospena@unibz.it

Peer-review under responsibility of the Gruppo Italiano Frattura (IGF)
doi:10.1016/j.proeng.2015.06.243

1. Introduction

A recent trend for the fabrication of more resistant and lightweight car body components is the usage of tailor welded blanks (TWBs) made of advanced high strength steels (AHSSs), such as dual phase, transformation-induced plasticity steels, hot stamping boron steels, and high strength low alloy steels. A tailor welded blank (TWB) is a single plane sheet that consists of two or more sheets that are welded together prior to the forming of the final component. Sheets are joined by laser welding and may have the same or different thicknesses, mechanical properties or surface coatings [1]. As a result, the formability of a TWB weld seam is notably influenced by many factors such as the material property variability in the heat-affected zone and fusion zone [2-6], the effects of the weldment on the strain distribution, failure site, crack propagation, and the non-uniform deformation also due to the differences in thickness properties, or surface [7-9]. Overall mechanical properties of welded joints are commonly evaluated by standard tensile tests, while local properties are based on microhardness tests. However, the occurrence of a weld seam in a TWB influences the distribution of strain field and, hence, the state of stress at local level during forming operation. Therefore, the possibility of measuring the full-field deformation of the weld seams gives a notable contribution in evaluating the mechanical behavior of the fusion zone and of the heat affected zone, as well as on their interaction with the parent metals.

In this work, a hot stamping boron steel, 22MNB5 grade, and a dual phase (DP) steel have been butt welded by a laser source in order to study the mechanical behavior of the weldment and of the region of the base metals affected from the heat input. Hourglass shaped specimens have been machined from the welded sheet to induce a higher deformation in the weld seam during standard tensile tests. Particularly, the weldment was placed transversally to the load direction along the minimum cross section. Digital images have been acquired during runs on both faces of the welded samples. Different cameras and lenses have been used, one framing the whole gauge area, and the other focusing on the welded part only. Digital image correlation [10-12] is used to analyze the deformation field on the metal surface, providing all the planar components of strain. Through thickness strain can be also evaluated, indirectly, assuming constant volume deformation. A post-processing strategy to tune the parameters of the algorithm of the DIC, and aimed at optimizing the digital image correlation capability to capture strain gradients induced by the laser welding is presented here. Finally, performances of the two setup arrangements, operating at different magnification levels, are highlighted.

2. Experimental setup

The experimental campaign has been carried out on hourglass shaped specimens, obtained by machining a DP-22MnB5 tailored blank. Table 1 summarizes the main mechanical properties of each material. Table 2 reports the geometrical dimensions of the samples.

Table 1. Principal properties of base materials.

Property	DP	22MnB5
σ_y (MPa)	470	1050
σ_u (MPa)	690	1440
Elongation at fracture (%)	19	5

Table 2. Specimen geometrical dimension.

Dimension	(mm)
Gauge section	12
Radius	50
Thickness DP	1.25
Thickness 22MnB5	1.00

Each specimen side is painted with a speckle pattern. Quasi-static tensile tests have been conducted using an

MTS hydraulic axial machine; load and displacement have been acquired during runs. Images acquisition is performed using two digital cameras, a Pixelink A781 and a Nikon D7000, each on one side of the specimen, mounted on rigid supports. The Pixelink sports a CMOS sensor with a resolution of 3000×2208 pixels whereas the Nikon is equipped with a 4928×3264 CMOS sensor. The first one has been used in conjunction with a 1:1 telecentric lens; the latter with a Nikkor 60 mm macro lens.

Time synchronization is provided among the two cameras and the data acquisition system of the axial machine. The D7000 has been set to frame the whole specimen, grabbing a picture every two seconds, while the Pixelink A781 framed a portion of the welded zone only, acquiring one picture per second. All images have been stored for subsequent DIC postprocessing. Several repetitions of the test showed a good repeatability of the results. Fig. 1 shows the load vs. displacement curve coming from one of the tests. The vertical coloured lines highlight four load levels as described hereafter. The highest level corresponds to the maximum load reached during the test.

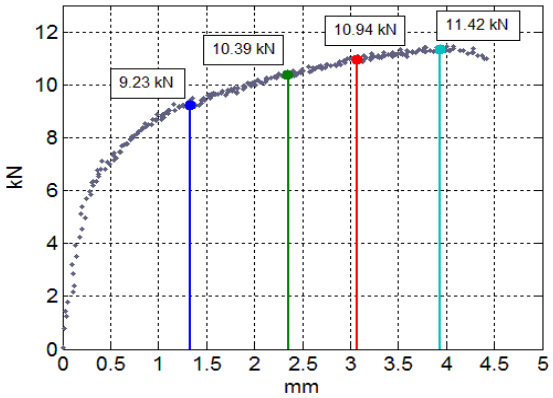

Fig. 1. DP-22MnB5 test: load-displacement curve.

3. Mechanical investigation through white light speckle image correlation

The strain measurement technique based on numerical correlation of white-light speckle images [10] may profitably be used to enquire the mechanical behavior of materials where the assessment of all strain components and their field distribution is particularly meaningful [12-14].

The entire procedure starts from the marking of specimen surface (on both faces) with a speckle pattern that can be easy attained by spray painting. Typically, the specimens are firstly covered by a fair layer of white paint for matting the specimen metallic surface, then, a quick wipe of black generates the wanted randomly spotted pattern.

During each test some hundred picture are grabbed and stored by the two cameras at their best allowed resolution. The analysis has been executed using an original image correlation method, developed by the authors [12, 13], and based on a ‘global approach’ that constrains the computed displacement field to be continuous across the entire images. The image field is divided into sub-images similarly to a plane element mesh in a finite element model. During the following image processing, it is required that the displacements of grid nodes (i.e. the sub-image vertex) accomplish a congruency constraint so that gaps or overlapping among elements (i.e. sub-images) are not possible.

Considering the correlation between two images, the displacement computation is carried out as follows: the first picture is divided into a grid of square sub-images that are the elements of the undeformed reference mesh. On the deformed image an analogous operation is performed, but here the node grid, although constrained to be continuous, is now allowed to be reshaped to follow the surface deformation.

The target of the global correlation algorithm is to arrange the nodes of the deformed grid so that the sub-images which comes from the resampling of the deformed image look like as close as possible to the corresponding sub-images of the reference image. Using a nonlinear least-squares approach, this problem is solved by minimizing the difference between the element sub-images in the two configurations moving the deformed grid nodes. At convergence, the displacement field is completely determined, and along the entire field, the strain components will

be computed by means of the Cauchy-Green theory for large strains description.

Sequentially the first image is correlated to the second, then to the third, and so on, using the previous step output as first guess for the next one.

Typically, each iteration takes less than one second on a common laptop computer. To process the initial images (when strains are small) a few iterations are sufficient to convergence, but, when the specimen is close to the final rupture and the grid is highly distorted, some tens of iteration are required to process each new image. As shown in the next section, the analysis output is given in terms of contour plots and time history of node data that are: the x and y displacements on sensor plane, the plane components of strains (ε_{xx}, ε_{yy}, γ_{xy}), the total equivalent strain and the through thickness strain computed indirectly, upon the constancy of volume hypothesis for plastic deformations.

Notice also that to follow the curved borders of hourglass shaped specimens, the image processing algorithm automatically discards all the grid elements that fall outside the speckle pattern, and elements that fall across the pattern border are masked so that only their valid fraction (where the speckle pattern is present) are further processed.

In the present analysis, considering the high strain gradients due to the weld seam and to the different mechanical properties of the two specimen halves, a special care has been given to choose the size of image subsets dimension. In fact, within each element the displacement field is modelled with a bilinear shape function, which may cancel strain peaks.

The pictures coming from the D7000 have allowed to be processed using subsets as small as 45×45 pixel (equivalent to 0.5×0.5 mm on specimen surface), instead the Pixelink sequence has been processed reducing element size from 1×1 mm down to 0.125×0.125 mm, that means from 210×210 to 35×35 pixel. The comparison among the different outputs (see next section, Fig. 9 and 10) has given important suggestions to optimize accuracy and sensitivity of the correlation algorithm.

4. Results and discussion

For both optical acquisition systems, the captured images have been processed to obtain the full-field strain distribution over the specimen surface.

The results obtained from the elaboration of images from Nikon camera are first presented, as contour maps and also graphs along the horizontal and vertical paths on the specimen as depicted in Fig. 2. In this figure, the red vertical line indicates the symmetry axis (vertical axis) of the specimen. The transverse red line (horizontal axis) labeled *0 mm* is placed on the weld seam; other horizontal paths are not equi-spaced due to the joint asymmetric behavior. All the results are relative to this reference system. More in details, the full-field equivalent strain and through thickness strain for the four load levels of Fig. 1 are shown in Fig. 3. From these data, the overall strain distribution over the surface of the gauge area of the specimen can be evaluated. The upper part, made of DP steel, undergoes the most severe plastic deformation, reaching a maximum value around 0.25; than necking and subsequent fracture occur. The other base material, the 22MnB5 steel, exhibits a very low deformation, due to higher mechanical properties with respect to the DP steel (Tab. 1). The welded part shows a limited deformation.

The same results are quantified along the abovementioned paths, and reported in Fig. 4 and 5. Each subplot represents one path, where every curve refers to a different load level.

Fig. 6 shows the total equivalent strain and the through thickness strain along the vertical path. As before, four curves are compared, one for each loading condition. The solid vertical grey line identifies the position of the weld seam. It is worth noting that the peak values are always localized about 5 mm above the welding, without any significant change in position over time.

Results from the acquisition system with the highest magnification are used to better investigate the strain gradients in the fusion and heat affected zones. To relate the post elaboration outcomes from the two cameras each frame of one side of the sample has to be matched with the corresponding one coming from the other side. To this purpose, five steps are necessary: time synchronization, magnification match, angular, vertical and horizontal alignment. Time synchro was ensured during test run. Angular alignment was checked during setup. Magnification matching was obtained during post processing: the telecentric lens ensured a 1:1 magnification ratio for Pixelink camera, while for the D7000 images the proper scaling factor was deduced from the dimensions of the undeformed clamping ends of the specimen. Vertical and horizontal alignments were found by matching the axes of the shear

distortion fields of the two sides, again using correlation techniques. Fig. 7 shows the quality of the resulting match, the small lighter rectangle, squared in red, being the frame coming from the Pixelink overlapped on the Nikon one.

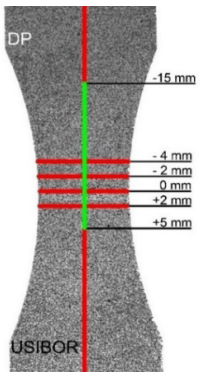

Fig. 2. True thickness strain at four load levels.

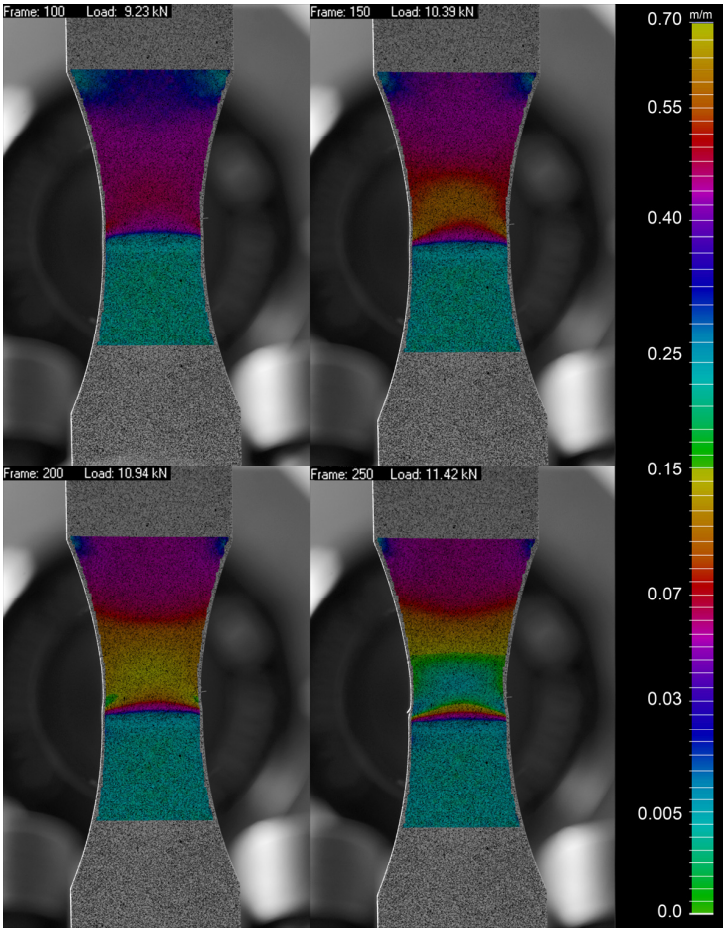

Fig. 3. Total equivalent strain at four load levels.

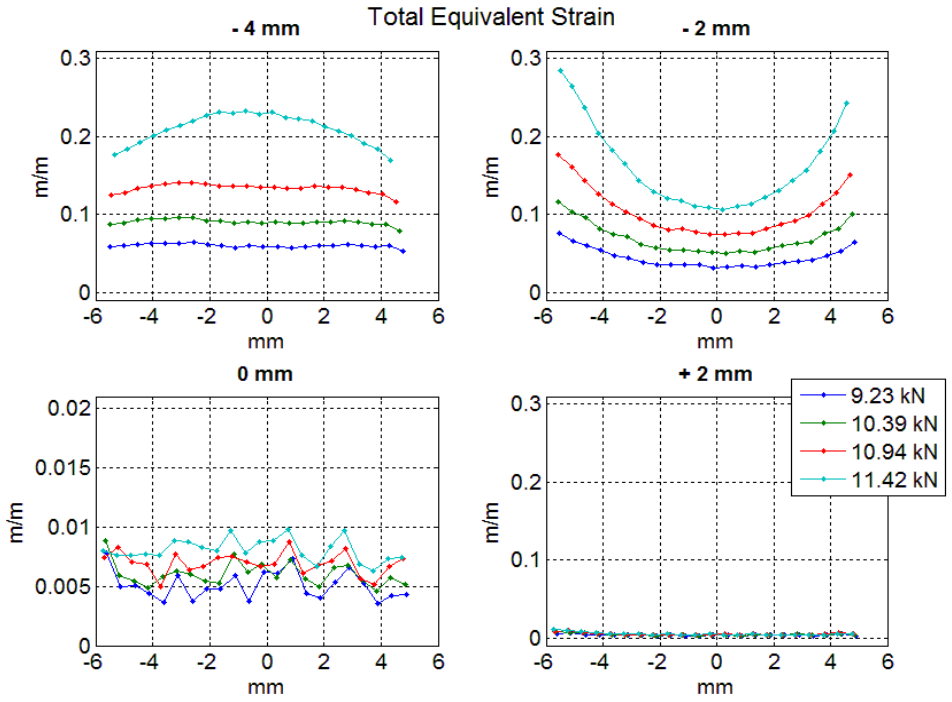

Fig. 4. Total equivalent strain at four different loads.

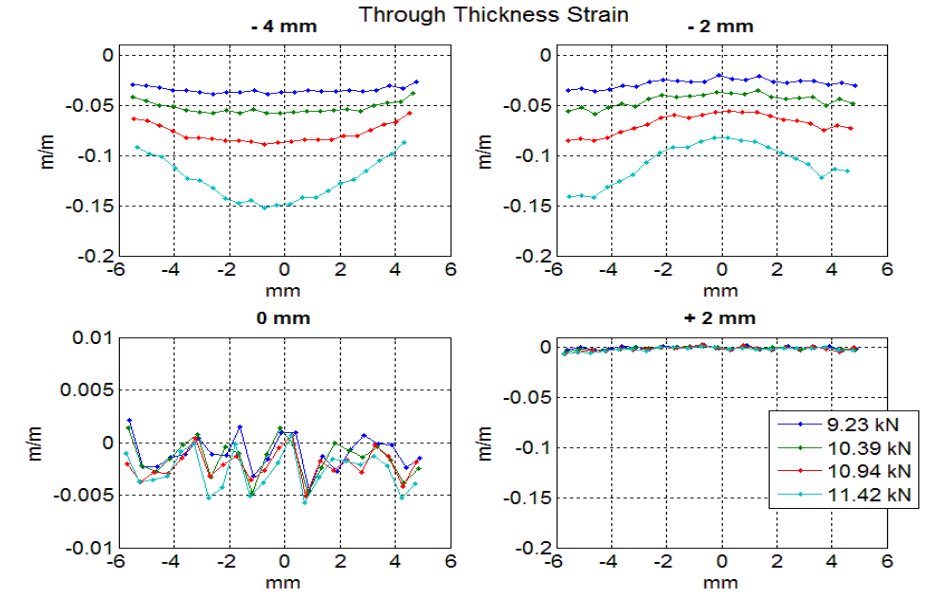

Fig. 5. Through thickness strain at four different loads.

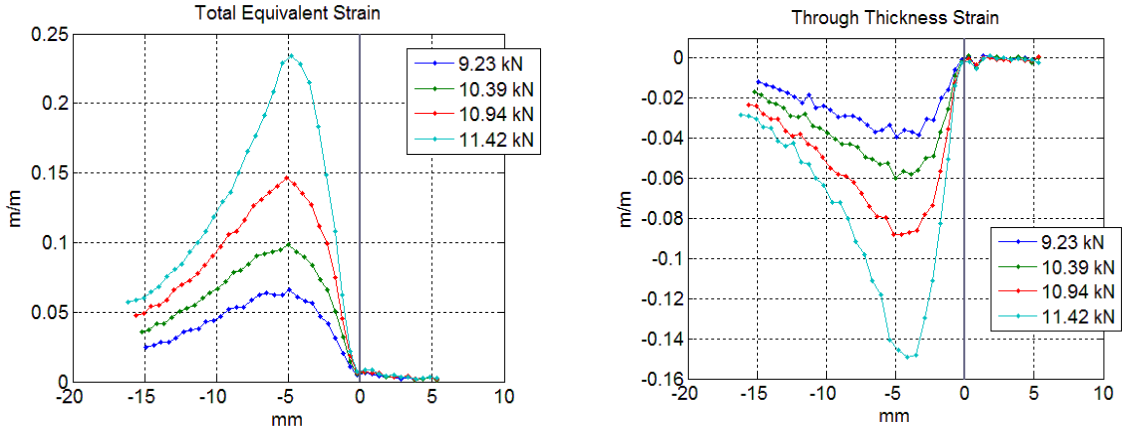

Fig. 6. Total equivalent strain and through thickness strain along the axial path.

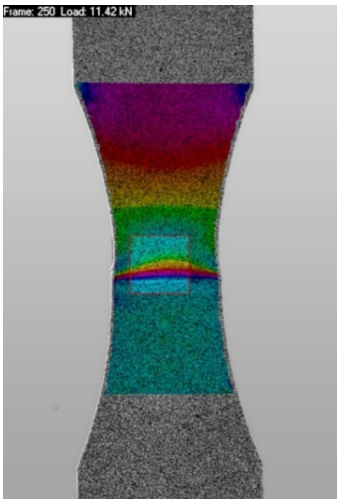

Fig. 7. Example of matching frames from the two cameras.

As mentioned before, Fig. 8 and 9 give a comparison among the post-processing outputs varying the size of sub-image grid. They show the equivalent and the through thickness strains along the specimen axis and across the weld seam. This path has been chosen because here the highest strain gradients are expected. It is clearly visible that using large subsets such as 2×2 mm wide (about two times the specimen thickness) returns erroneous results both in terms of gradient (too much smooth) and maximum strains (too small). Similarly, the outcome of the smallest used grid (0.125×0.125 mm on Pixelink images) shows a scattered behavior most likely caused by image noise.

On the contrary, comparing 0.5×0.5 mm grids on both cameras, we got very similar results that let us to highlight the important results that the measured values are not depending on patterns, grabbing hardware or subset sizes (in terms of pixels). Also, image processing at higher resolutions (possible only on Pixelink images) only slightly improves strain gradient depiction close to the seam (around -1 mm on plots).

This confirms that the use of two cameras on both specimen faces is possible and useful, and that a high resolution sensor (such as the Nikon one) is enough to inquire the strain field around welded joints and that the use of a second camera focused on the seam could help to detect strain irregularities or singularities if a quite higher magnification is chosen.

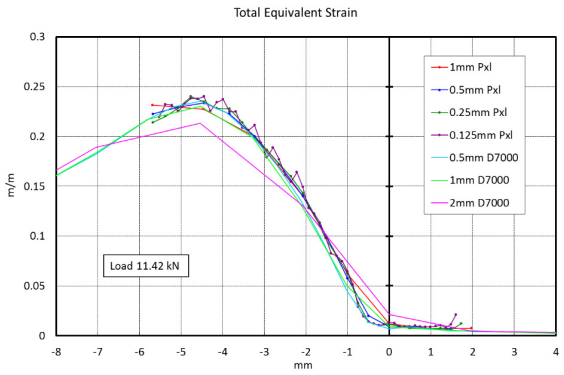

Fig. 8. Comparison between total equivalent strain curves obtained from different cameras using different subset sizes.

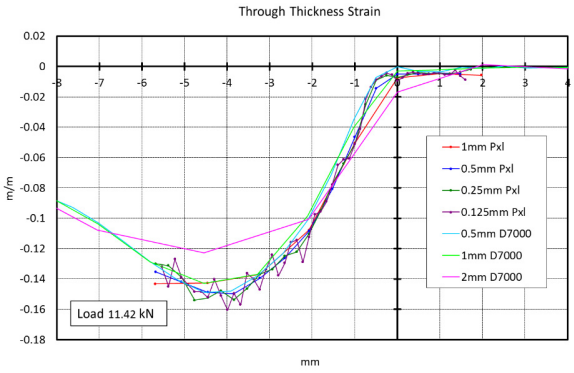

Fig. 9. Comparison between through thickness strain curves obtained from different cameras using different subset sizes.

References

[1] Auto/Steel Partnership: Tailor Welded Blank Design and Manufacturing Manual, Technical Report, 1995.
[2] B. Kinsey, Z. Liu, J. Cao, A novel forming technology for tailor welded blanks, J. Mater. Process. Technol. 99 (2000) 145-153.
[3] N. Sreenivasan, M. Xia, S. Lawson, Y. Zhou, Effect of laser welding on formability of DP980 steel, J. Eng. Mater. Technol. (Trans. ASME) 130 (2008) 0410041–0410049.
[4] M. Xia, N. Sreenivasan, S. Lawson, Y. Zhou, A comparative study of formability of diode laser welds in DP980 and HSLA steels, J. Eng. Mater Technol. (Trans. ASME) 129 (2007) 446-452.
[5] S.K. Panda, N. Sreenivasan, M. Kuntz, Y. Zhou, Numerical simulation and experimental results of tensile test behavior of laser butt welded DP980 steel, J. Eng. Mater. Technol. (Trans. ASME) 130 (2008) 041003-041011.
[6] D. Dry, W. Wadell, D.R.J. Owen, Determination of laser weld properties for finite element analysis of laser welded tailored blanks, Sci. Technol. Weld. Join. 7 (2002) 11-18.
[7] C.H. Cheng, M. Jie, C.L. Chan, C.L. Chow, True stress–strain analysis on weldment of heterogeneous tailor-welded blanks - a novel approach for forming simulation, Int. J. Mech. Sci. 49 (2007) 217-229.
[8] G. Kridli, P.A. Friedman, A.M. Sherman, Formability of aluminum tailor welded blanks, SAE Technical Paper No. 2000-01-0772 (2000) 1-9.
[9] L.C. Chan, S.M. Chan, C.H. Cheng, T.C. Lee, Formability and weld zone analysis of tailor-welded blanks for various thickness ratios, J. Eng. Mater. Technol. 127 (2005) 179-185.
[10] P. Cheng, M.A. Sutton, H.W. Schreier, S.R. McNei, Full-field speckle pattern image correlation with b-spline deformation function, Exp. Mech. 42 (2002) 344-352.
[11] F. Hild, S. Roux, Displacement measurement to identification of elastic properties – a review, Strain 42 (2006) 69-80.
[12] G.B. Broggiato, L. Cortese, White-light speckle image correlation applied to large-strain material characterization, Eur. J. Comput. Mech. 18 (2009) 377-392.
[13] G.B. Broggiato, L. Casarotto, Z. Del Prete, D. Maccarrone, Full-field strain rate measurement by white-light speckle image correlation, Strain 45 (2009) 364-372.
[14] G.B. Broggiato, F. Campana, L. Cortese, E. Mancini, Comparison between two experimental procedures for cyclic plastic characterization of high strength steel sheets, J. Eng. Mat. Tech. (Trans. ASME), 134 (2012) 63-72.